

# Joint clustering with alignment for temporal data in a one-point-per-trajectory setting

Polina ARSENTEVA<sup>1</sup>, Mohamed Amine BENADJAOUD<sup>2</sup> and Hervé CARDOT<sup>1</sup>

*1) Institut de Mathématiques de Bourgogne, UMR CNRS 5584,*

*Université de Bourgogne, Dijon, France*

*2) IRSN PSE-SANTE/SERAMED, Fontenay aux roses, France*

November 20, 2023

## Abstract

Temporal data, obtained in the setting where it is only possible to observe one time point per trajectory, is widely used in different research fields, yet remains insufficiently addressed from the statistical point of view. Such data often contain observations of a large number of entities, in which case it is of interest to identify a small number of representative behavior types. In this paper, we propose a new method performing clustering simultaneously with alignment of temporal objects inferred from these data, providing insight into the relationships between the entities. A series of simulations confirm the ability of the proposed approach to leverage multiple properties of the complex data we target such as accessible uncertainties, correlations and a small number of time points. We illustrate it on real data encoding cellular response to a radiation treatment with high energy, supported with the results of an enrichment analysis.

**Key words:** Complex temporal data, k-medoids clustering, multivariate statistics.

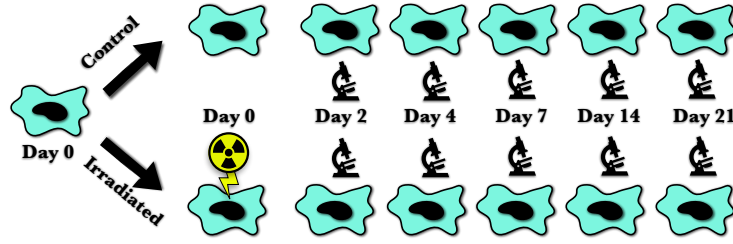


Figure (1.1) A schematic representation of the experimental design used to obtain the data motivating this paper. Transcriptional profiles of human endothelial cells were measured with real-time qPCR under control and under a single irradiation dose of 20 Gy at 0 h using a linear particle accelerator (LINAC) at 4 MV, 2.5 Gy/min, at 2, 4, 7, 14 and 21 days.

# 1 Introduction

Temporal data are omnipresent in various domains of research in biology, physics, econometrics, and many others. Among them we encounter cases where longitudinal data are observed on the same individuals. Statistical inference in these cases can be addressed by such frameworks as functional data analysis (Ramsay and Silverman, 2005), time series and Gaussian process inference (Rasmussen and Williams, 2005). However, in many studies measurements for different time points cannot be performed on the same individuals. For example, the aforementioned context is common in biology, including in vitro studies, requiring such destructive measurements as real-time qPCR or microarray (e.g. Gomez-Cabrero et al. (2019); Luo et al. (2023); Sifakis et al. (2011)), and in vivo, where the sacrifice of the animal is often necessary (e.g. Bertho et al. (2020); Hu et al. (2023); Kuballa et al. (2011)).

This paper is motivated by an in vitro experiment studying the response of human endothelial cells to irradiation with a high energy level. Figure 1.1 schematically represents the experimental setting. Since the interest lies in studying the dynamic of the response to the considered treatment, multiple time points are measured. Due to the destructive nature of the measurements, compromising the cells and making them unsuitable for repeated measurements, every time point is observed on a separate culture flask. This implies that we do not have access to temporal correlations in the dataset, and cannot observe an actual temporal signal and treat the data as time series. In practice, cellular populations used

to take measurements for each time point are separated from one population just prior to the experiments. Therefore, the flasks used for different time points contain different cells, which implies that we can reasonably assume the independence with respect to the temporal dimension.

Datasets considered in this paper share a number of other characteristics that contribute to their complexity and lead to a non-trivial statistical problem. One important characteristic is the presence of two conditions, in which case the focus is put on studying the differences in response between the two conditions. In case of experimental studies, two conditions, referred to as case (treated) and control (non-treated), are necessary to study the effect of the treatment of interest. In the example presented on Figure 1.1, these treatment conditions are irradiated and non-irradiated. The information on both conditions can be encoded in a fold change, representing the difference between the corresponding responses. Fold changes are widely used in biology, but are generic by definition and can be applied in different fields, for example in econometrics, where a similar concept is referred to as "treatment effect" (Wooldridge, 2010).

Furthermore, multiple replicates are necessary in order to account for measurement uncertainties, which is especially crucial given that different time points are observed independently. In this case, the mean values over replicates represent an actual signal, but should not be considered alone for the inference since this does not include the information on uncertainties. Consequently, the inference approach has to take into account the available information on uncertainties and cross section correlations between entities. This implies the insufficiency of simple techniques such as treating only mean signals, which is what we observe in literature in the context of clustering performed on such data (e.g. Dang et al. (2017); Kuballa et al. (2011); Ren et al. (2022); Sifakis et al. (2011); Shahid et al. (2019)). The uncertainties are generally only taken into account purely for visualization purposes of a small number of entities (e.g. Dang et al. (2017); Luo et al. (2023); Shahid et al. (2019); Ren et al. (2022)).

Finally, the goal in such studies is to evaluate the response of multiple entities, whose number is often significantly larger than that of time points that are the same for all entities, making functional data analysis and stochastic process-based approaches unsuitable for inference. The analysis in such cases usually involves reducing the datasets to a small number of groups characterized by typical behavior templates, which methodologically translates into the task of clustering. Additional information on the joint distribution of entities is often available through the data and has to be accounted for. For instance, the data used as an example in this work is transcriptomic, which means that the expression of up to multiple hundreds of genes is measured. For a given experimental condition and time point, the measurements for all genes are taken simultaneously from the cells of one culture flask, providing access to correlations between the genes. Additionally, in many cases there exists prior knowledge on underlying causal relationships between the considered entities. In this respect, the temporal aspect of the data can be leveraged by integrating the alignment into clustering, thus on the one hand aiding the clustering itself, and on the other hand gaining information on the predictive nature of the entities. A number of approaches performing joint clustering with alignment exist in the framework of functional data analysis (e.g. [Sangalli et al. \(2010\)](#); [Cremona and Chiaromonte \(2023\)](#)) and (e.g. [Kazlauskaite et al. \(2019\)](#)), which, while not adapted for dealing with the data targeted in this paper, will serve as inspiration for the proposed approach.

In this work, we propose a statistical framework that addresses these challenges, while leveraging data characteristics to render the computations time efficient. In [Section 2](#), we introduce estimators of fold changes as well as a new distance, accounting for the information on uncertainties and cross section correlations that is available in the considered datasets. We present a multivariate computationally efficient procedure performing simultaneous alignment and clustering of the fold changes based on the constructed distance. We choose the framework of clustering with k-medoids ([Kaufmann and Rousseeuw, 1987](#)), since it is based on comparing elements to a medoid, a representative element of the given cluster that is

an actual member of the population. The latter distinguishes k-medoids from k-means and many other clustering methods, and ensures a number of important properties, such as the ability to keep track of correlations throughout clustering, and the possibility of rendering alignment clustering-dependent. The proposed approach is evaluated in the framework of multiple simulation studies in Section 3 in comparison with a number of alternative choices. Finally, in Section 4 we present an application to the data acquired in the radiobiological experimental setting presented earlier. The obtained information is validated through the bioinformatic enrichment analysis of the clusters.

## 2 Materials and methods

### 2.1 Fold change modeling and estimation

In the multivariate setting, in order to avoid introducing non-existent information by smoothing the temporal response, we consider time as discrete. For a given dataset, we define the response variable as  $Y_{ikj}^t$  for an entity (gene)  $i \in \{1, 2, \dots, n_e\}$ , under the experimental condition  $k = 0$  if control (non-irradiated) and  $k = 1$  if case (irradiated), at a time point  $t \in \{t_1, t_2, \dots, t_p\}$  and for a replicate  $j \in \{1, 2, \dots, n_r\}$ . Here we assume there are  $n_r$  observations for both experimental condition and every time point without loss of generality, given that  $n_r \geq 2$ .

Two constraints with respect to the covariances between the responses follow from the specificity of the experimental design. On the one hand, the measures of expressions for all genes for a given experimental condition and time point are collected from the same plate, which allows to estimate cross section covariances between genes, i.e.  $\text{Cov}(Y_{ikj}^t, Y_{i'kj}^t)$  for  $i \neq i'$ . On the other hand, we do not have access to the temporal covariance structure due to the destructive technique used in collecting measures from a plate for a given time point. Thus, measures for different time points are produced individually on different cells and are not correlated, i.e. given distinct time points  $t \neq t'$ , for any replicate pair  $(j, j') \in \{1, 2, \dots, n_r\}^2$

and entity pair  $(i, i') \in \{1, 2, \dots, n_e\}^2$  we have  $\text{Cov}(Y_{ikj}^t, Y_{i'kj'}^{t'}) = 0$ .

Classical estimators of the fold changes in the multivariate setting are the pointwise estimators: a set of empirical individual fold changes is denoted by  $\Gamma = (\Gamma_1, \dots, \Gamma_{n_e})$  where  $\Gamma_i = (\Gamma_i^{t_1}, \dots, \Gamma_i^{t_p})$  such that  $\Gamma_i^t = \frac{\sum_{j=1}^{n_r} Y_{i1j}^t - \sum_{j=1}^{n_r} Y_{i0j}^t}{n_r} = \overline{Y_{i1}^t} - \overline{Y_{i0}^t}$ , representing the difference between the means of the control and the case response. However, these estimators do not take into account the information of uncertainties and correlations present in the data. We propose a new definition of fold changes estimators in order to fully take into account all the information about their estimated distributions:

**Definition 2.1.** *The estimator of the fold change of entity  $i$  is denoted by  $\widehat{\Gamma}_i$ , assumed to be a random Gaussian vector and is defined as  $\widehat{\Gamma}_i | \Gamma_i, \Sigma_{\Gamma_i} \sim \mathcal{N}(\Gamma_i, \Sigma_{\Gamma_i})$  where  $\Gamma_i^t = \overline{Y_{i1}^t} - \overline{Y_{i0}^t}$  (the pointwise estimator), and  $\Sigma_{\Gamma_i}$  is a diagonal matrix with the diagonal  $(\sigma_{\Gamma_i^{t_1}}^2, \dots, \sigma_{\Gamma_i^{t_p}}^2)$  such that  $\sigma_{\Gamma_i^t}^2 = \frac{\sum_{j=1}^{n_r} [(Y_{i1j}^t - \overline{Y_{i1}^t})^2 + (Y_{i0j}^t - \overline{Y_{i0}^t})^2]}{n_r - 1}$ .*

**Remark 2.1.** *The fact that the covariance matrix in Definition 2.1 is diagonal is a direct consequence of the second covariance constraint mentioned above.*

## 2.2 Introducing a new distance between fold change estimators

Since the task at hand is clustering of the estimators of fold changes, and thus distribution clustering, there is a need to choose an appropriate distance. First, we expand the Definition 2.1 to a pair of fold changes by specifying their joint distribution:

**Definition 2.2.** *The estimator of a pair of fold changes of entities  $i$  and  $i'$  is denoted as  $[\widehat{\Gamma}_i^\top \widehat{\Gamma}_{i'}^\top]^\top$ , assumed to be a random Gaussian vector and is defined as follows:*

$$\begin{bmatrix} \widehat{\Gamma}_i \\ \widehat{\Gamma}_{i'} \end{bmatrix} \sim \mathcal{N} \left( \begin{bmatrix} \Gamma_i \\ \Gamma_{i'} \end{bmatrix}, \begin{bmatrix} \Sigma_{\Gamma_i} & P_{\Gamma_i \Gamma_{i'}} \\ P_{\Gamma_i \Gamma_{i'}}^\top & \Sigma_{\Gamma_{i'}} \end{bmatrix} \right),$$

where the quantities  $\Gamma_i$ ,  $\Gamma_{i'}$ ,  $\Sigma_{\Gamma_i}$  and  $\Sigma_{\Gamma_{i'}}$  describing marginal distributions of  $\widehat{\Gamma}_i$  and  $\widehat{\Gamma}_{i'}$  are

defined according to Definition 2.1, and the diagonal cross-covariance matrix  $P_{\Gamma_i \Gamma_{i'}}$  with the diagonal  $(\rho_{\Gamma_i \Gamma_{i'}^{t_1}}, \dots, \rho_{\Gamma_i \Gamma_{i'}^{t_p}})$  such that  $\rho_{\Gamma_i \Gamma_{i'}^{t_l}} = \frac{\sum_{j=1}^{n_r} [(Y_{i1j}^t - \overline{Y_{i1}^t})(Y_{i'1j}^t - \overline{Y_{i'1}^t}) + (Y_{i0j}^t - \overline{Y_{i0}^t})(Y_{i'0j}^t - \overline{Y_{i'0}^t})]}{n_r - 1}$ .

The chosen distance is constructed based on  $L^2$ -distance between normally distributed fold changes estimators  $\widehat{\Gamma}_i$  and  $\widehat{\Gamma}_{i'}$ , the latter is constructed as  $d_2^2(\widehat{\Gamma}_i, \widehat{\Gamma}_{i'}) = \mathbb{E} \|\widehat{\Gamma}_i - \widehat{\Gamma}_{i'}\|_2^2 = \|\Gamma_i - \Gamma_{i'}\|_2^2 + \text{Tr}(\Sigma_{\Gamma_i}) + \text{Tr}(\Sigma_{\Gamma_{i'}}) - 2\text{Tr}(P_{\Gamma_i \Gamma_{i'}})$  where  $\|\cdot\|_2$  is the the Euclidean norm (Givens and Shortt, 1984).

**Definition 2.3.** The squared  $L^2$ -distance between fold changes estimators  $\widehat{\Gamma}_i$  and  $\widehat{\Gamma}_{i'}$ , with the joint distribution given in Definition 2.2, will be denoted as  $\widehat{\mathbf{d}}_2^2$  and defined as follows:

$$\widehat{\mathbf{d}}_2^2(\widehat{\Gamma}_i, \widehat{\Gamma}_{i'}) = \sum_{l=1}^p (\Gamma_i^{t_l} - \Gamma_{i'}^{t_l})^2 + \sum_{l=1}^p \sigma_{\Gamma_i^{t_l}}^2 + \sum_{l=1}^p \sigma_{\Gamma_{i'}^{t_l}}^2 - 2 \sum_{l=1}^p \rho_{\Gamma_i \Gamma_{i'}^{t_l}}.$$

## 2.3 Fold change alignment

In this section, we introduce all the mathematical quantities necessary to perform the temporal alignment of the fold changes, which will be further applied jointly with clustering. The idea behind alignment is illustrated in Figure 2.1. In this example, fold changes are very similar up to a time shift, which means that alignment should significantly reduce the distance between them and thus force them to belong to the same cluster. First, we define a transformation of a pair of time vectors that will be referred to as a time warp, in analogy with a similar concept in functional data analysis.

**Definition 2.4.** Let  $\mathcal{T}$  and  $\mathcal{T}_s$  be sets of time vectors for considered omic datasets. A time warp  $\mathcal{W}_s$  of step  $s \in \mathbb{Z}$  is a transformation of two time vectors, defined as follows:

$$\mathcal{W}_s: \mathcal{T}^2 \rightarrow \mathcal{T}_s^2$$

$$\begin{pmatrix} \mathbf{t}^0 \\ \mathbf{t}^0 \end{pmatrix} \mapsto \begin{pmatrix} \mathbf{t}^{11} \\ \mathbf{t}^{12} \end{pmatrix} \text{ where:}$$

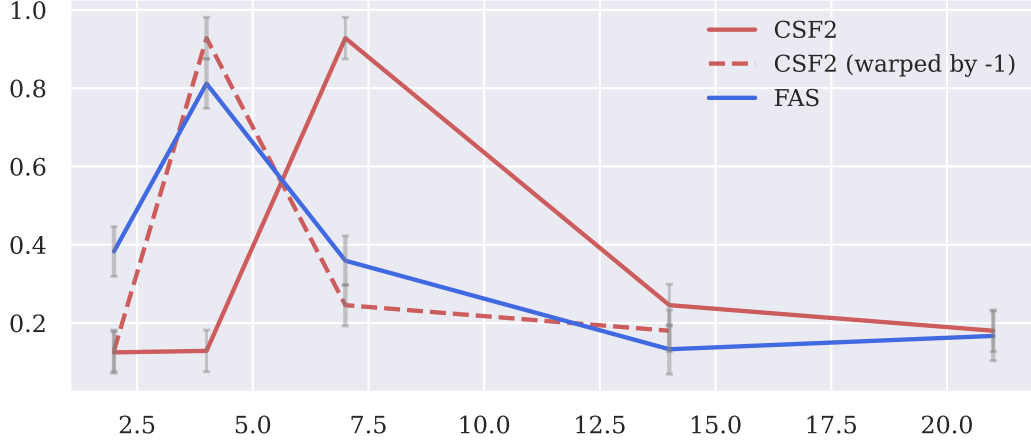


Figure (2.1) The effect of time warping illustrated on a figure, where means with standard deviation of a pair of normalized transcriptomic fold changes are plotted. It can be observed that after warping the fold change of the gene CSF2 backwards (continuous line represents the original mean and the dashed one represents the warped mean), its mean practically coincides with that of the fold change of the gene FAS.

$$\mathbf{t}^0 = \{t_l\}_{l=1}^p, \quad \mathbf{t}^{11} = \begin{cases} \{t_l\}_{l=1}^{p-s} & \text{if } s > 0 \\ \{t_l\}_{l=1-s}^p & \text{if } s < 0 \\ \mathbf{t}^0 & \text{if } s = 0 \end{cases} \quad \text{and} \quad \mathbf{t}^{12} = \begin{cases} \{t_l\}_{l=1+s}^p & \text{if } s > 0 \\ \{t_l\}_{l=1}^{p+s} & \text{if } s < 0 \\ \mathbf{t}^0 & \text{if } s = 0 \end{cases}.$$

In this definition, we distinguish three major warping types: backward warp ( $s < 0$ ), forward warp ( $s > 0$ ) and identity warp ( $s = 0$ ). Next, we define a warped fold changes pair in terms of the original fold changes:

**Definition 2.5.** Let  $\mathbf{t}^0 \in \mathcal{T}$  be a  $p$ -dimensional time vector, and  $s \in \mathbb{Z}$  a warp step. We denote as  $\left[\widehat{\Gamma_i \circ \mathcal{W}_s}^\top \widehat{\Gamma_{i'} \circ \mathcal{W}_s}^\top\right]^\top$  an  $s$ -warped fold changes pair  $\left[\widehat{\Gamma_i}^\top \widehat{\Gamma_{i'}}^\top\right]^\top$  such that:

$$\begin{bmatrix} \widehat{\Gamma_i \circ \mathcal{W}_s} \\ \widehat{\Gamma_{i'} \circ \mathcal{W}_s} \end{bmatrix} = \begin{bmatrix} \left(\widehat{\Gamma_i}^{\mathbf{t}^1_1}, \dots, \widehat{\Gamma_i}^{\mathbf{t}^1_{p-|s|}}\right)^\top \\ \left(\widehat{\Gamma_{i'}}^{\mathbf{t}^1_{p-|s|+1}}, \dots, \widehat{\Gamma_{i'}}^{\mathbf{t}^1_{p-(p-|s|)}}\right)^\top \end{bmatrix} \quad \text{where } \mathbf{t}^1 = \mathcal{W}_s(\mathbf{t}^0).$$

**Remark 2.2.** In order to be able to refer directly to an individual warped fold change, we denote it as  $\widehat{\Gamma_i \circ \mathcal{W}_s}$  with a slight abuse of notation, since the warping transformation is



applied to a pair of fold changes.

For every fold changes pair only the first fold change is being moved since it allows for a more convenient manipulation of warping results while being able to examine all warping possibilities if considering both forward and backward type warping. According to the definitions presented above, the first fold change in the pair is being warped with a subsequent cutoff of extraneous parts. The second fold change in the pair does not move, however its parts that do not correspond to remaining post-warping points of the first one are also being cut off. The calculations are detailed in the proof of Proposition 2.1.

We introduce a new dissimilarity measure between the random fold changes estimators that is a generalization of the distance  $\widehat{\mathbf{d}}_2^2$  in order to take all the covariances into account in the case where time warping is applied:

**Definition 2.6.** Let  $s \in \mathbb{Z}$ , and  $X$  and  $Y$  be  $p$ -dimensional Gaussian random variables with a joint distribution

$$\begin{bmatrix} X \\ Y \end{bmatrix} \sim \mathcal{N} \left( \begin{bmatrix} \mu_X \\ \mu_Y \end{bmatrix}, \begin{bmatrix} \Sigma_X & \mathbf{P}_{XY} \\ \mathbf{P}_{XY}^\top & \Sigma_Y \end{bmatrix} \right) \text{ such that } [\mathbf{P}_{XY}]_{ij} = 0 \text{ if } j \neq i - s.$$

We define a dissimilarity measure  $\widehat{\mathbf{diss}}_s$  between  $X$  and  $Y$  as follows:

$$\widehat{\mathbf{diss}}_s(X, Y) = \|\mu_X - \mu_Y\|^2 + \text{Tr}(\Sigma_X) + \text{Tr}(\Sigma_Y) - 2 \sum_{l=1}^{p-|s|} [\mathbf{P}_{XY}]_{(l+s\mathbb{1}_{\mathbb{Z}_+^*}(s), l+s\mathbb{1}_{\mathbb{Z}_-^*}(s))}.$$

Applying the dissimilarity measure to the warped fold changes, we get the expression resembling the value of  $\widehat{\mathbf{d}}_2^2$  in the case of non-warped fold changes, with extraneous part getting cut off as a result of warping:

**Proposition 2.1.** Let  $s \in \mathbb{Z}$  be a warp step, and  $\left[ \widehat{\Gamma_i \circ \mathcal{W}_s}^\top \widehat{\Gamma_{i'} \circ \mathcal{W}_s}^\top \right]^\top$  an  $s$ -warped fold changes pair. The value of dissimilarity  $\widehat{\mathbf{diss}}_s$  between the fold changes  $\widehat{\Gamma_i \circ \mathcal{W}_s}$  and  $\widehat{\Gamma_{i'} \circ \mathcal{W}_s}$

can be expressed in the following form:

$$\widehat{\text{diss}}_s \left( \widehat{\Gamma_i \circ \mathcal{W}_s}, \widehat{\Gamma_{i'} \circ \mathcal{W}_s} \right) = \sum_{l=l^*}^{p^*} \left( \Gamma_i^{t_l} - \Gamma_{i'}^{t_{l+s}} \right)^2 + \sum_{l=l^*}^{p^*} \sigma_{\Gamma_i^{t_l}}^2 + \sum_{l=l^*}^{p^*} \sigma_{\Gamma_{i'}^{t_{l+s}}}^2 - 2 \sum_{l=1+|s|}^{p-|s|} \rho_{\Gamma_i \Gamma_{i'}^{t_l}},$$

where  $l^* = 1 - s\mathbb{1}_{\mathbb{Z}_-}(s)$  and  $p^* = p - s\mathbb{1}_{\mathbb{Z}_+}(s)$ .

**Remark 2.3.** It can be noted that  $\widehat{\text{diss}}_s \left( \widehat{\Gamma_i \circ \mathcal{W}_s}, \widehat{\Gamma_{i'} \circ \mathcal{W}_s} \right) = \widehat{\mathbf{d}}_2^2 \left( \widehat{\Gamma}_i, \widehat{\Gamma}_{i'} \right)$  in the case of the identity warp  $s = 0$ .

**Remark 2.4.** We chose to construct time warping in a way that some parts of the fold changes that move outside of the temporal domain considered, get cut off. This choice was deemed as preferable to alternatives based on extending the fold changes instead of cutting them, since they imply adding unobserved information. However, it potentially introduces a bias in comparison between warped and unwarped sequences, hence it is important to normalize the dissimilarities with respect to the number of post-warping time points in order to render them comparable (implemented in our package *ScanOFC*).

## 2.4 Joint clustering with alignment

The main idea behind our approach to key features selection for a given dataset is reducing the fold changes to a small number of behavior types up to a time shift, which translates into clustering of aligned fold changes. In order to combine dissimilarities between fold changes with optimal alignments, we introduce the following matrix:

**Definition 2.7.** Let  $\mathcal{S} = \{-s_{\max}, \dots, s_{\max}\} \subset \mathbb{Z}$  be a finite set of allowed warp steps, given a maximal warping step  $s_{\max} \in \mathbb{N}$ . The Optimal Warping Dissimilarity matrix, denoted  $\mathcal{OWD}$ , is a matrix containing the values of the dissimilarity measure  $\widehat{\text{diss}}_s$  for all pairs of fold changes in case of their optimal pairwise alignment over the set of all possible warps

---

**Algorithm 1** Joint clustering and alignment algorithm: classical version
 

---

**Require:** Fold changes  $\hat{\Gamma} = (\hat{\Gamma}_1, \dots, \hat{\Gamma}_{n_e})$ ,  $K \in \mathbb{N}$ ,  $it_{max} \in \mathbb{N}$ ,  $n_{init} \in \mathbb{N}$ ,  $\epsilon > 0$ .

```

1:  $TC \leftarrow \infty$ 
2: for  $init \in \{1, \dots, n_{init}\}$  do
3:   Initialize centroids  $C = (C_1, \dots, C_K) \subset \{1, \dots, n_e\}$  with kmeans++
4:    $TC_{it} \leftarrow \infty$ 
5:    $\Delta TC \leftarrow \infty$ 
6:    $it \leftarrow 1$ 
7:   while  $\Delta TC > \epsilon$  and  $it < it_{max}$  do
8:      $TC_{it}^{new} \leftarrow 0$ 
9:     1. Assign step:
10:    for  $i \in \{1, \dots, n_e\}$  do
11:       $d_{min} \leftarrow \infty$ 
12:      for  $k \in \{1, \dots, K\}$  do
13:         $s_k \leftarrow \arg \min_{s \in S} \widehat{\text{diss}}_s \left( \widehat{\Gamma_i \circ \mathcal{W}_s}, \widehat{\Gamma_{C_k} \circ \mathcal{W}_s} \right)$  ▷ Align FCs with the centroid
14:         $d_k \leftarrow \widehat{\text{diss}}_{s_k} \left( \widehat{\Gamma_i \circ \mathcal{W}_{s_k}}, \widehat{\Gamma_{C_k} \circ \mathcal{W}_{s_k}} \right)$ 
15:        if  $d_k < d_{min}$  then ▷ Assign FCs to centroids
16:           $d_{min} \leftarrow d_k$ 
17:           $Cl_i \leftarrow k$ 
18:        end if
19:      end for
20:    end for
21:    2. Update step:
22:    for  $k \in \{1, \dots, K\}$  do
23:       $d_{min} \leftarrow \infty$ 
24:      for  $i \in cluster_k = \{i \in \{1, \dots, n_e\} | Cl_i = k\}$  do ▷ Candidate for a centroid
25:         $d_{cluster_k} \leftarrow 0$ 
26:        for  $i' \in cluster_k$  do
27:           $s_{i'i} \leftarrow \arg \min_{s \in S} \widehat{\text{diss}}_s \left( \widehat{\Gamma_{i'} \circ \mathcal{W}_s}, \widehat{\Gamma_i \circ \mathcal{W}_s} \right)$  ▷ Align FCs with the candidate
28:           $d_{cluster_k} \leftarrow d_{cluster_k} + \widehat{\text{diss}}_{s_{i'i}} \left( \widehat{\Gamma_{i'} \circ \mathcal{W}_{s_{i'i}}}, \widehat{\Gamma_i \circ \mathcal{W}_{s_{i'i}}} \right)$ 
29:        end for
30:        if  $d_{cluster_k} < d_{min}$  then ▷ Choose new centroid
31:           $d_{min} \leftarrow d_{cluster_k}$ 
32:           $C_k^{new} \leftarrow i$ 
33:        end if
34:      end for
35:       $TC_{it}^{new} \leftarrow TC_{it}^{new} + d_{min}$ 
36:    end for
37:    3. Calculate the change in total cost:
38:     $\Delta TC \leftarrow TC_{it} - TC_{it}^{new}$ 
39:    if  $\Delta TC > \epsilon$  then
40:       $C \leftarrow (C_1^{new}, \dots, C_K^{new})$ 
41:       $TC_{it} \leftarrow TC_{it}^{new}$ 
42:    end if
43:     $it \leftarrow it + 1$ 
44:  end while
45:  if  $TC_{it} < TC$  then
46:     $C \leftarrow (C_1, \dots, C_K)$  ▷ centroids labels
47:     $Cl \leftarrow (Cl_1, \dots, Cl_{n_e})$  ▷ cluster labels
48:     $\mathcal{W} \leftarrow (s_{1Cl_1}, \dots, s_{n_e Cl_{n_e}})$  ▷ warps
49:     $TC \leftarrow TC_{it}$ 
50:  end if
51: end for
52: return  $C, Cl, \mathcal{W}$ 

```

---

with steps in  $\mathcal{S}$ , or formally:

$$\mathcal{OWD} = \left[ \min_{s \in \mathcal{S}} \left[ \widehat{\text{diss}}_s \left( \widehat{\Gamma_i \circ \mathcal{W}_s}, \widehat{\Gamma_{i'} \circ \mathcal{W}_s} \right) \right] \right]_{1 \leq i, i' \leq n_e}.$$

---

**Algorithm 2** Joint clustering and alignment algorithm based on  $\mathcal{OWD}$  and  $\mathcal{OW}$  matrices

---

**Require:** Fold changes  $\hat{\Gamma} = (\hat{\Gamma}_1, \dots, \hat{\Gamma}_{n_e})$ ,  $K \in \mathbb{N}$ ,  $it_{max} \in \mathbb{N}$ ,  $n_{init} \in \mathbb{N}$ ,  $\epsilon > 0$ .

```

1: Compute  $\mathcal{OWD}$  and  $\mathcal{OW}$ 
2:  $TC \leftarrow \infty$ 
3: for  $init \in \{1, \dots, n_{init}\}$  do
4:   Initialize centroids  $C = (C_1, \dots, C_K) \subset \{1, \dots, n_e\}$  with kmeans++
5:    $TC_{it} \leftarrow \infty$ 
6:    $\Delta TC \leftarrow \infty$ 
7:    $it \leftarrow 1$ 
8:   while  $\Delta TC > \epsilon$  and  $it < it_{max}$  do
9:      $TC_{it}^{new} \leftarrow 0$ 
10:    1. Assign step:
11:    for  $i \in \{1, \dots, n_e\}$  do
12:       $Cl_i \leftarrow \arg \min_{k \in \{1, \dots, K\}} \mathcal{OWD}_{iC_k}$  ▷ Assign aligned FCs to centroids
13:    end for
14:    2. Update step:
15:    for  $k \in \{1, \dots, K\}$  do
16:       $d_{min} \leftarrow \infty$ 
17:      for  $i \in cluster_k = \{i \in \{1, \dots, n_e\} | Cl_i = k\}$  do ▷ Candidate for a centroid
18:         $d_{cluster_k} \leftarrow \sum_{i' \in cluster_k} \mathcal{OWD}_{ii'}$ 
19:        if  $d_{cluster_k} < d_{min}$  then ▷ Choose new centroid
20:           $d_{min} \leftarrow d_{cluster_k}$ 
21:           $C_k^{new} \leftarrow i$ 
22:        end if
23:      end for
24:       $TC_{it}^{new} \leftarrow TC_{it}^{new} + d_{min}$ 
25:    end for
26:    3. Calculate the change in total cost:
27:     $\Delta TC \leftarrow TC_{it} - TC_{it}^{new}$ 
28:    if  $\Delta TC > \epsilon$  then
29:       $C \leftarrow (C_1^{new}, \dots, C_K^{new})$ 
30:       $TC_{it} \leftarrow TC_{it}^{new}$ 
31:    end if
32:     $it \leftarrow it + 1$ 
33:  end while
34:  if  $TC_{it} < TC$  then
35:     $C \leftarrow (C_1, \dots, C_K)$  ▷ centroids labels
36:     $Cl \leftarrow (Cl_1, \dots, Cl_{n_e})$  ▷ cluster labels
37:     $\mathcal{W} = (\mathcal{OW}_{1Cl_1}, \dots, \mathcal{OW}_{n_e Cl_{n_e}})$  ▷ warps
38:     $TC \leftarrow TC_{it}$ 
39:  end if
40: end for
41: return  $C, Cl, \mathcal{W}$ 

```

---

According to Definition 2.4, alignments are uniquely defined not for a given fold change, but for a given pair of fold changes. In other words, a fold change may have different optimal

warps when paired with different fold changes, and thus the elements of the  $OWD$  matrix are not directly comparable. Hence, the task can only be approached by iterating between clustering and alignment until convergence. Using k-medoids allows to make alignment clustering-dependent: while comparing elements to medoids for clustering, their warps can also be chosen in a unique way with respect to medoids. In comparison, many other methods such as k-means or its extensions are unsuitable for the task. For example, k-means applied directly to the  $OWD$  matrix is potentially applicable, but it is not suitable for alignment since it does not allow to choose fold change warps uniquely. Another option could be performing k-means through constructing a fold change barycenter, which is unsuitable since the barycenters are not observed from the data, and after the first iteration the information on joint distributions is lost.

We perform clustering using "k-means like" version of k-medoids (Park and Jun, 2009) based on a series of random initializations of type k-means++ (Arthur and Vassilvitskii, 2007). Pseudocode for the state-of-the-art version of joint clustering and alignment, applied in the context discussed in this work, is presented in Algorithm 1. We propose a modification of the algorithm, that reduces the computation time by leveraging the low temporal dimensionality of the data in the multivariate setting. Since the number of time points is typically small, the number of possible warps has to be even smaller and known in advance, and since the distributions of the fold change pairs under different warps are known, it is possible to calculate all alignment options before performing clustering, while reducing computation time and in a non-memory-intensive way. Consequently, we introduce the following quantity, that will be used in the modified version of the algorithm:

**Definition 2.8.** *Let  $\mathcal{S} = \{-s_{max}, \dots, s_{max}\} \subset \mathbb{Z}$  be a finite set of allowed warp steps, given a maximal warping step  $s_{max} \in \mathbb{N}$ . The Optimal Warp matrix, denoted  $OW$ , is a matrix containing, for all pairs of fold changes, the values in  $\mathcal{S}$  corresponding to the warp steps allowing to achieve their optimal pairwise alignment with respect to the dissimilarity*

measure  $\widehat{\mathbf{diss}}_s$ , or formally:

$$\mathcal{OW} = \left[ \arg \min_{s \in \mathcal{S}} \left[ \widehat{\mathbf{diss}}_s \left( \widehat{\Gamma_i \circ \mathcal{W}_s}, \widehat{\Gamma_{i'} \circ \mathcal{W}_s} \right) \right] \right]_{1 \leq i, i' \leq n_e}.$$

**Proposition 2.2.** *The following statements are true for matrices  $\mathcal{OWD}$  and  $\mathcal{OW}$ :*

1.  $\mathcal{OWD}$  is symmetric.
2.  $\mathcal{OW}$  is anti-symmetric.

**Remark 2.5.**  $\mathcal{OW}$  allows to interpret the main warping types. For a given fold changes pair, if the optimal warp is the identity warp, they are referred to as simultaneous. If not, then one fold change in the pair is warped forward with respect to the other, whereas the other fold change is being warped backwards with respect to the first. In this case, the fold change that is warped forward is referred to as 'predictive' of other one, whereas the latter is labeled as 'predicted', or 'regulated'.

The modified version of the previous algorithm, presented in Algorithm 2, is based on integrating time warping in the clustering process through pre-calculated matrices  $\mathcal{OWD}$  and  $\mathcal{OW}$ . The former replaces a standard dissimilarity matrix, the latter is used to extract final warps. The comparison between the two algorithms leads to the following result:

**Theorem 2.1.** *The following is true about the joint clustering and alignment algorithms:*

1. Algorithm 2 converges in a finite number of iterations.
2. Algorithms 1 and 2 are equivalent, in the sense that for the same input they produce the same output.
3. Algorithms 1 and 2 have polynomial time complexities, that are given in the proof. Moreover, the degree of the largest polynomials of the time complexity of Algorithm 1 is greater than that of Algorithm 2, meaning that the latter is less complex.

**Remark 2.6.** *In practice, the improvement of Algorithm 2 in terms of the runtime can be very important because a large value often has to be chosen for  $n_{init}$ . Since such clustering algorithms tend to be rather initialization sensitive, it is beneficial to perform such a number of random initializations that covers a sufficiently big range of initial combinations, which becomes important with higher values of  $n_e$ .*

**Remark 2.7.** *In line 37 of Algorithm 2, the indexing order of  $\mathcal{OW}$  is important, since this matrix is anti-symmetric, as shown in Proposition 2.1. This specific indexing implies that the fold changes are being warped with respect to their centroids, which remains static.*

## 2.5 Sign penalty

The following feature is motivated by the fact that, in terms of interpretation, there is an important difference between positively and negatively expressed fold changes. As a means to reinforce this distinction in the obtained clusters, we introduce a penalty term that increases the dissimilarity for those pairs of entities with different signs for one or more corresponding instances. For a warp step  $s$  and entity index pair  $(i, i') \in \{1, \dots, n_e\}^2$ , the penalty term represents the proportion of time points where the means of the two considered fold changes have different signs:

$$Pen\left(\widehat{\Gamma_i \circ \mathcal{W}_s}, \widehat{\Gamma_{i'} \circ \mathcal{W}_s}\right) = \frac{1}{p - |s|} \sum_{l=1}^{p-|s|} \mathbb{1}_{\mathbb{R}_-} \left( (\Gamma_i \circ \mathcal{W}_s)_{t_l} \times (\Gamma_{i'} \circ \mathcal{W}_s)_{t_l} \right).$$

By analogy with the distance matrix, a penalty matrix can be formulated:

$$[Pen_{ii'}]_{1 \leq i, i' \leq n_e} \text{ such that } Pen_{ii'} = Pen\left(\widehat{\Gamma_i \circ \mathcal{W}_s}, \widehat{\Gamma_{i'} \circ \mathcal{W}_s}\right).$$

Finally, the penalized dissimilarity is defined with a penalization hyperparameter  $\lambda \geq 0$ :

$$Pen\left(d\left(\widehat{\Gamma_i \circ \mathcal{W}_s}, \widehat{\Gamma_{i'} \circ \mathcal{W}_s}\right)\right) = \widehat{\text{diss}}_s\left(\widehat{\Gamma_i \circ \mathcal{W}_s}, \widehat{\Gamma_{i'} \circ \mathcal{W}_s}\right) + \lambda \times Pen_{ii'}.$$

This penalized dissimilarity is integrated into the aligned clustering procedure by replacing  $\widehat{\text{diss}}_s \left( \widehat{\Gamma_i \circ \mathcal{W}_s}, \widehat{\Gamma_{i'} \circ \mathcal{W}_s} \right)$  in Definitions 2.7 and 2.8.

### 3 Simulation study

A series of simulation studies was performed in order to evaluate the proposed methodology in the framework similar to that of temporal fold changes with respect to the existing state-of-the-art alternatives. In every scenario,  $n_e = 300$  fold changes were simulated over  $p = 8$  time points ranging from 0.5 to 21. Simulated fold changes are defined by their means and their covariance matrix. Using the same notation as previously in the context of real datasets, let the means be represented by  $\Gamma = (\Gamma_1, \dots, \Gamma_{n_e})$ , where  $\Gamma_i = (\Gamma_i^{t_1}, \dots, \Gamma_i^{t_p})$  for  $i \in \{1, \dots, n_e\}$ . The covariance matrices will be denoted by  $\Psi = (\Psi_{ii'})_{(i,i') \in \{1, \dots, n_e\}^2}$ , where  $\Psi_{ii'}$  is a diagonal matrix, with the diagonal  $(\psi_{\Gamma_i \Gamma_{i'}^{t_1}}, \dots, \psi_{\Gamma_i \Gamma_{i'}^{t_p}})$ , such that, for  $t \in \{t_1, \dots, t_p\}$ ,  $\psi_{\Gamma_i \Gamma_{i'}^t} = \sigma_{\Gamma_i^t}^2$  if  $i = i'$ , and  $\psi_{\Gamma_i \Gamma_{i'}^t} = \rho_{\Gamma_i \Gamma_{i'}^t}$  otherwise. The differences in the design of different scenarios are presented in Table 3.1.

	Nb. of clusters	$\Gamma_i$ distribution	$\Psi'_{ii'}$ distribution	$f_\Psi$
<b>M1-C1</b>	4	$\mathcal{U}(\{f_1, f_2, f_3, f_4\})$	$\mathcal{N}(0, 2^2)$ if $i = i'$ , 0 otherwise	$f_\Psi = id$
<b>M1-C2</b>	2	$\mathcal{U}(\{f_1, f_2\})$	$\mathcal{N}(0, 2^2)$ if $i = i'$ , 0 otherwise	$f_\Psi = id$
<b>M1-C3</b>	2	$\mathcal{U}(\{f_1, f_2\})$	$ \mathcal{N}(0, 2^2) $ if $\mathbb{1}_{cl_1}(i) = \mathbb{1}_{cl_1}(i')$ , 0 otherwise	$f_\Psi(x) = \frac{x^2}{cst_1}$
<b>M1-C4</b>	2	$\mathcal{U}(\{f_1, f_2\})$	$ \mathcal{N}(0, 2^2) $ if $\mathbb{1}_{cl_1}(i) = \mathbb{1}_{cl_1}(i')$ , 0 otherwise	$f_\Psi(x) = \frac{x^2}{cst_2}$
<b>M1-C5</b>	2	$\mathcal{U}(\{f_1, f_2\})$	$\mathcal{U}([0, 1])$ if $\mathbb{1}_{cl_1}(i) = \mathbb{1}_{cl_1}(i') = 1, \mathcal{U}([-1, 0])$ if $\mathbb{1}_{cl_2}(i) = \mathbb{1}_{cl_2}(i') = 1, 0$ otherwise	$f_\Psi(x) = \frac{x^2}{cst_3}$
<b>M1-C6</b>	2	$\mathcal{U}(\{f_1, f_2\})$	$\mathcal{U}([0, 1])$ if $\mathbb{1}_{cl_1}(i) = \mathbb{1}_{cl_1}(i') = 1, \mathcal{U}([-1, 0])$ if $\mathbb{1}_{cl_2}(i) = \mathbb{1}_{cl_2}(i') = 1, 0$ otherwise	$f_\Psi(x) = \frac{x^2}{cst_4}$
<b>M2</b>	4	$\mathcal{U}(\{f_1, f_2, f_3, f_4\})$	$\mathcal{N}(0, 2^2)$ if $i = i'$ , 0 otherwise	$f_\Psi = id$

Table (3.1) Details on the simulation design in all scenarios, denoted by codes, such that M1 and M2 indicate two different approaches to the simulation of means, and C1-C6 indicate different ways to simulate covariances. The covariances are defined through a matrix and a scaling transformation:  $\Psi_{ii'} = f_\Psi(\Psi'_{ii'})$ . The scaling constants are set as follows:  $\{cst_1, cst_2, cst_3, cst_4\} = \{\max\{\psi'_{\Gamma_i \Gamma_{i'}^t} | i \neq i', t \in \{t_1, \dots, t_p\}\}, 20, 100, 50\}$ .



The design of the fold change means is detailed in Table 3.2. It can be noted that the means were simulated based on 4 behavior types that were meant to reproduce the characteristics of the real fold changes similar to those observed on real data. The simulations are characterized by a relatively low level of model-imposed features. In particular, we only assume that the fold changes have estimated probability distributions described by means and covariances, thus we simulate directly the fold changes estimators. The temporal complexity of the data is independent of the framework we propose, and is only inspired by the functional patterns we observe in real data.

	<b>M1</b>	<b>M2</b>
<b>Cluster 1</b>	$f_1(x) = \frac{a}{2}x^2 + bx + c$	$f_1(x) = \frac{a}{2}(x - s)^2 + b(x - s) + c$
<b>Cluster 2</b>	$f_2(x) = \frac{a}{3}x^3 - \frac{a(r_1+r_2)}{2}x^2 + (ar_1r_2 + c)x + d$	$f_2(x) = \frac{a}{3}(x - s)^3 - \frac{a(r_1+r_2)}{2}(x - s)^2 + (ar_1r_2 + c)(x - s) + d$
<b>Cluster 3</b>	$f_3(x) = \frac{a}{3}x^3 - \frac{a(r_1+r_2)}{2}x^2 + (ar_1r_2 + c)x + d$	$f_3(x) = \frac{a}{3}(x - s)^3 - \frac{a(r_1+r_2)}{2}(x - s)^2 + (ar_1r_2 + c)(x - s) + d$
<b>Cluster 4</b>	$f_4(x) = \frac{a}{4}x^4 - \frac{a(r_1+r_2+r_3)}{3}x^3 + \frac{a(r_1r_2+r_3(r_1+r_2))}{2}x^2 - (ar_1r_2r_3 + b)x + c$	$f_4(x) = a \sin(b(x - s)) + c$

Table (3.2) Distributions of the simulated fold change means for each of the 4 behavior types (clusters) in 2 different scenarios. Every simulated fold change is an independent realization of one of these templates, with all the coefficients being random (Gaussian or uniform). In particular,  $s$  is the time shift parameter appearing only in the second simulation study M2, with the distribution  $s \sim \mathcal{U}([-7, 7])$ . A continuous distribution is chosen since in real life time shifts can be reasonably assumed to be continuous, which cannot be captured since we only have access to measurements at discrete time points.

The first simulation study (scenarios M1-C1 to M1-C6) focuses on the evaluating different distances and clustering algorithms. Attempting to mimic the real data as closely as possible, the time points were spaced in the same way as in of of the real omic datasets:  $(t_1, \dots, t_p) = (0.5, 1, 2, 3, 4, 7, 14, 21)$ . The study confirmed the superiority of performing  $\widehat{\mathbf{d}}_2^2$ -based k-medoids on fold changes-like data<sup>1</sup>. In particular, the success of  $\widehat{\mathbf{d}}_2^2$  k-medoids

<sup>1</sup>See Supplementary Figure C.1 for details.

compared to Wasserstein k-means and hierarchical clustering within the independent scenarios M1-C1 and M1-C2 demonstrates that k-medoids algorithm is more adapted to perform clustering of fold changes. The remaining scenarios incorporating different levels of intra-cluster covariances show that  $\widehat{\mathbf{d}}_2^2$  manages to leverage the correlations for clustering more successfully than Wasserstein or Hellinger distances.

The second simulation study (scenario M2) is aimed at evaluating the effect of integrating time warping into clustering. Here the time points were set almost equally spaced, with the goal of correcting the important changes in scale arising from the horizontal shifts of the fold changes applied in order to study the effect of alignment:  $(t_1, \dots, t_p) = (0.5, 3, 6, 9, 12, 15, 18, 21)$ . Since the approach remains non-functional, it does not affect the interpretability of the findings.

	Without alignment		With alignment	
	$\mathcal{D}$ -based k-medoids	$\mathcal{D}$ -based spectral clustering	$\mathcal{OWD}$ -based k-medoids	$\mathcal{OWD}$ -based spectral clustering
<b>Mean ARI</b>	0.22	0.26	0.61	0.26
<b>Mean V-measure</b>	0.39	0.45	0.67	0.47

Table (3.3) Results of the simulation study of the effect of incorporating time warping into clustering. Standard deviations of the ARI (Chacón and Rastrojo, 2023) and V-measure (Rosenberg and Hirschberg, 2007) scores are 0.04 for the  $\mathcal{D}$ -based k-medoids, and of order  $10^{-3}$  and less for the rest of the methods.

The results of this simulation study are presented in Table 3.3. We compared the proposed algorithms performing k-medoids clustering jointly with alignment to k-medoids clustering without alignment, more specifically applied to the distance matrix  $\mathcal{D}$  containing observed distances instead of post-warping ones. We also tested spectral clustering with and without aligning, applied to the dissimilarity matrices transformed into similarity matrices with a transformation  $f(\mathcal{M}) = \frac{\max \mathcal{M} - \mathcal{M}}{\max \mathcal{M}}$  for a given matrix  $\mathcal{M}$ . The spectral clustering algorithm (von Luxburg, 2007) was performed using the framework implemented in Python package *scikit-learn*, which consists in performing k-means clustering on relevant eigenvectors of a

normalized Laplacian matrix of the similarity matrix. On the one hand, the study demonstrated the interest of integrating time warping in order to take temporal shifts into account. On the other hand, using the example of spectral clustering, often being preferred to k-medoids, the study showed that the specific k-medoids based clustering framework proposed in this paper leverages the information on the alignments for clustering much better than other state-of-the-art clustering approaches applied on the same dissimilarity matrix  $OWD$ .

## 4 Application to real data

We demonstrate the proposed approach on real data from an in vitro study taking place in the radiobiological context, with the goal of assessing the effect of irradiation with higher energy level on human endothelial cells (HUVEC) through their transcriptomic expression. This study is a part of a research project initiated at the French Radioprotection and Nuclear Safety Institute (IRSN) that seeks to improve our knowledge on the adverse effects induced by radiotherapy on healthy tissues, with potential applications in clinical setting. The transcriptomic fold changes of 157 genes, measured at 2, 4, 7, 14 and 21 days after irradiation, were estimated based on 3 replicates from the log-transformed data according to the procedure presented in Section 2.1. We also preprocessed the fold changes in order to amplify more significant values and reduce the difference in scale effect, the details are presented in Appendix B. We performed clustering coupled with alignment based on the sign-penalized optimal warping dissimilarity matrix.

The five clusters<sup>2</sup> that were obtained are presented in Figure 4.1. The number of clusters was set at five since this is the smallest one allowing for a sufficient separation of features from the radiobiological point of view. The colorcode and the legend on the plots allow to identify which warp group (warped backward with respect to the centroid, simultaneous with the centroid and warped forward with respect to the centroid) each gene belongs to. The

---

<sup>2</sup>These plots only contain the means of preprocessed fold changes, giving a rough idea of the genes' behavior but can be at times misleading since clustering is performed on full fold changes, containing not only means but all the information on correlations and uncertainties that can be inferred from the replicates.

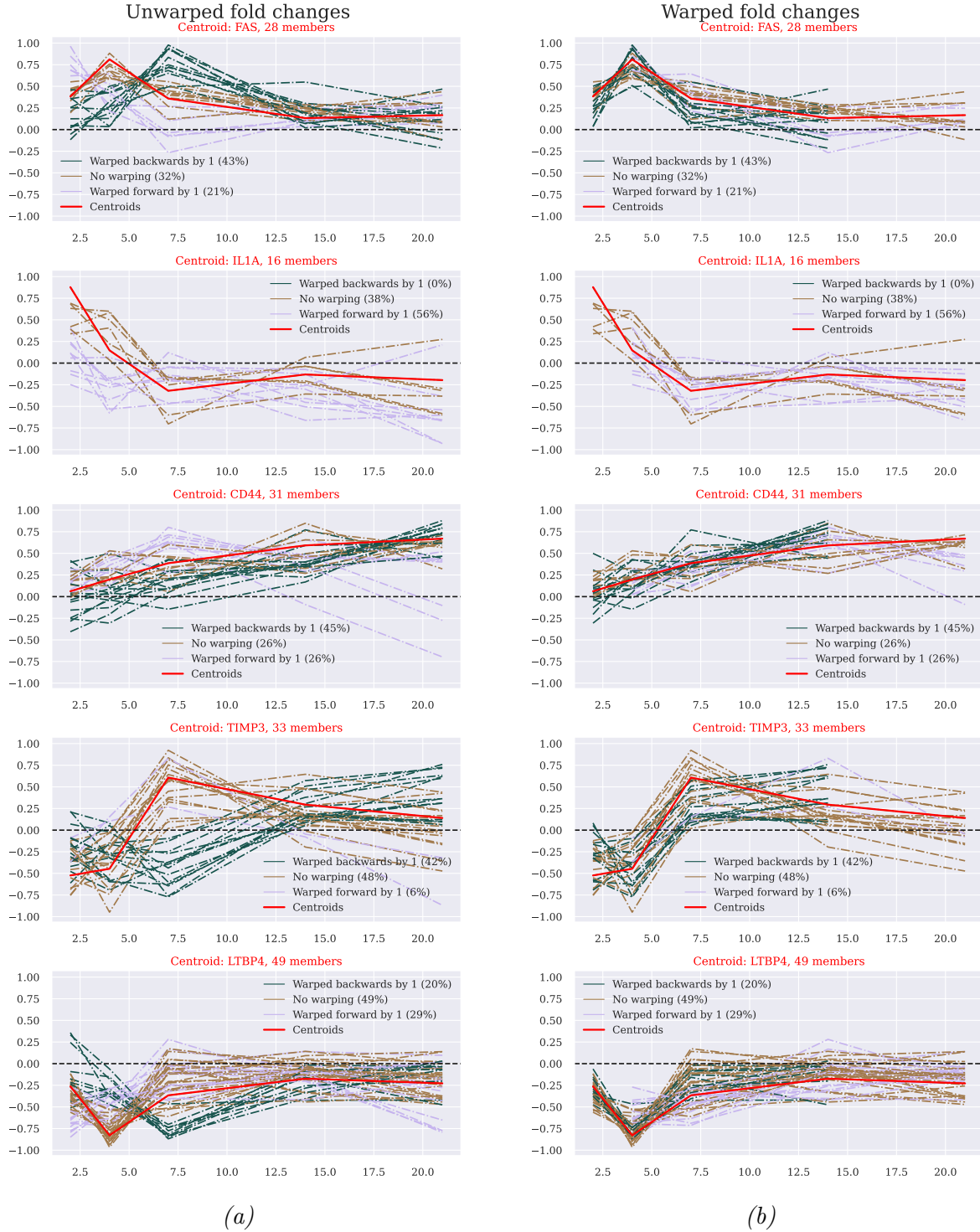


Figure (4.1) Clustering of the LINAC dataset with OWD-based  $k$ -medoids in 5 clusters. a) Means of original normalized fold changes (unaligned). b) Means of warped normalized fold changes (aligned).

aligned version is the one used for clustering, allowing to identify global behavior types up to a time shift, whereas the unaligned version allows to identify temporal cascades inside every cluster, i.e. the forward-warped predict simultaneous that predict the backward-warped. As a result, five distinct behavior types have been identified (top to bottom): up-regulated and tending towards zero, up-regulated initially and down-regulated later on, steady growth, down-regulated initially and up-regulated later on, down-regulated and tending towards zero. The clusters will be hereafter referred to by numbers according to this order. In comparison, spectral clustering on the similarity constructed from the  $OWD$  matrix, was also performed on this data in the same manner as on simulated data in the previous section. The obtained behavior types are much less distinguishable<sup>3</sup>, which is also confirmed by the silhouette score (Rousseeuw, 1987): 0.36 for our k-medoids-based approach against 0.24 for spectral clustering.

In order to gain insight into the biological interpretation of the quantities and patterns identified using our methodology, we performed the enrichment analysis of clusters with cellular processes using Pathway Studio. As a result of this analysis, for a list of genes contained in the given cluster, we obtained the cellular processes matching with an important proportion of these genes according to literature, and for each cellular process a subset of implicated genes, as well as some statistics such as the associated p-value. The considered processes were filtered out with respect to the p-value at the level of 0.01, and with respect to the overlap at the level that was chosen in order to get a sufficient amount of information for larger clusters and avoid getting excessive information for smaller clusters. The barplot with all of the detected cellular processes and their distributions across clusters is presented in Appendix, Figure C.4.

It can be observed that a number of processes are highly represented in multiple clusters, it is the case for example of cell proliferation and adhesion. We are particularly interested in those that are highly represented in only one cluster and not the others, thus allowing

---

<sup>3</sup>See Supplementary Figure C.3 for a visualization of the clusters.

to conclude that the cellular process in question potentially characterize this cluster. The identified cluster-specific cellular processes are consistent with the biological expectations. The up-regulated clusters 1 and 3 are shown to be associated respectively with cellular aging and oxidative stress. Indeed, both functions are related to senescence/apoptosis (Pole et al., 2016), and the implicated genes are expected to be significantly up-regulated under high energy irradiation. Moreover, 80% of genes from cluster 1 that were shown to be associated with cellular aging are either forward-warped or simultaneous, corresponding to an early expression pattern. This indicates the additional predictive potential of warp groups identified within given clusters. On the other hand, the genes from cluster 3 that have been linked to oxidative stress demonstrate stable growth in expression, peaking in the late phase, that may have been influenced by the aforementioned genes from cluster 1.

The genes from cluster 5, which has a down-regulated pattern symmetrically to cluster 1, are associated with cell survival. This function is of opposing nature with respect to apoptosis, and the corresponding genes are expected to show strong down-regulation in this context. The remaining clusters are of mixed nature and are more complex to analyze. Cluster 2 is the smallest in size and appears to contain mainly genes with endothelium-specific functions. Lastly, cluster 4 has been matched with DNA replication. The early down-regulation with a subsequent up-regulation of these genes is consistent with the idea of the DNA replication process initially slowing down as a reaction to stress, and being reinforced further on in order to restore the damaged tissues.

## 5 Discussion

In this article we propose a novel procedure designed for complex temporal data in the context when only one time point can be observed per trajectory. We designed a computationally efficient algorithm performing clustering jointly with temporal alignment of the fold changes, chosen as the object encoding the response in the context of two different treatment

groups. Our approach to modeling the fold changes as well as the proposed distance, with a further generalization to a dissimilarity measure, as well as the main algorithm have been shown to be better adapted for the treated setting than a number of alternative options. Moreover, having applied our method to real transcriptomic data, we managed to uncover biologically meaningful groups of genes with interpretable patterns. The proposed approach could potentially be extended to a more sophisticated form of clustering that may produce even better results on complex data.

## Software availability

Python package and the LINAC data are freely available at <https://github.com/parsenteva/scanofc>.

## Acknowledgments

We thank Olivier Guipaud, Fabien Milliat and Vincent Paget for the experimental data and useful discussions. This work is supported by the European Union through the PO FEDER-FSE Bourgogne 2014/2020 programs as part of the project ModBioCan2020, and by Institut de Radioprotection et de Sûreté nucléaire as part of the project ROSIRIS.

*Conflict of Interest:* none declared.

## References

- D. Arthur and S. Vassilvitskii. k-means++: the advantages of careful seeding. In *Proceedings of SODA*, pages 1027–1035. 2007.
- A. Bertho, et al. Preclinical Model of Stereotactic Ablative Lung Irradiation Using Arc Delivery in the Mouse: Effect of Beam Size Changes and Dose Effect at Constant Collimation. *Internat. J. Radiat. Oncol. Biol. Phys.*, 107(3):548–562. 2020.

- J. E. Chacón and A. I. Rastrojo. Minimum adjusted Rand index for two clusterings of a given size. *Adv Data Anal Classif*, 17(1):125–133. 2023.
- M. A. Cremona and F. Chiaromonte. Probabilistic K-mean with local alignment for clustering and motif discovery in functional data. *Journal of Computational and Graphical Statistics*, 32(3):1119–1130. 2023.
- L. Dang, et al. Dynamic Changes in the Splenic Transcriptome of Chickens during the Early Infection and Progress of Marek’s Disease. *Sci. Rep.*, 7. 2017.
- C. R. Givens and R. M. Shortt. A class of Wasserstein metrics for probability distributions. *Michigan Mathematical Journal*, 31(2):231–240. 1984.
- D. Gomez-Cabrero, et al. STATegra, a comprehensive multi-omics dataset of B-cell differentiation in mouse. *Sci Data*, 6(1):256. 2019.
- S. Hu, et al. Inferring circadian gene regulatory relationships from gene expression data with a hybrid framework. *BMC Bioinformatics*, 24(1):362. 2023.
- L. Kaufmann and P. Rousseeuw. Clustering by Means of Medoids. *Data Analysis based on the L1-Norm and Related Methods*, pages 405–416. 1987.
- I. Kazlauskaitė, et al. Gaussian Process Latent Variable Alignment Learning. In *Proceedings of AISTATS*, pages 748–757. 2019.
- A. V. Kuballa, et al. Moulting cycle specific differential gene expression profiling of the crab *Portunus pelagicus*. *BMC Genomics*, 12(1):147. 2011.
- Y. Luo, et al. Aloe-emodin inhibits African swine fever virus replication by promoting apoptosis via regulating NF- $\kappa$ B signaling pathway. *Virol J*, 20(1):158. 2023.
- H.-S. Park and C.-H. Jun. A simple and fast algorithm for K-medoids clustering. *Expert Systems with Applications*, 36(2, Part 2):3336–3341. 2009.



- A. Pole, et al. Oxidative stress, cellular senescence and ageing. *AIMS MOLES*, 3(3):300–324, 2016.
- J. Ramsay and B. W. Silverman. *Functional Data Analysis*. Springer Science & Business Media. 2005.
- C. Rasmussen and C. Williams. *Gaussian Processes for Machine Learning*. Adaptive Computation and Machine Learning series. MIT Press, 2005.
- Z.-M. Ren, et al. Comparative transcriptome and metabolome analyses identified the mode of sucrose degradation as a metabolic marker for early vegetative propagation in bulbs of *Lycoris*. *The Plant Journal*, 112(1):115–134, 2022.
- A. Rosenberg and J. Hirschberg. V-Measure: A Conditional Entropy-Based External Cluster Evaluation Measure. In *Proceedings of EMNLP-CoNLL*, pages 410–420. 2007.
- P. J. Rousseeuw. Silhouettes: A graphical aid to the interpretation and validation of cluster analysis. *J. Comput. Appl. Math.*, 20:53–65. 1987.
- L. M. Sangalli, et al. k-mean alignment for curve clustering. *Computational Statistics & Data Analysis*, 54(5):1219–1233. 2010.
- M. Shahid, et al. Comparative Transcriptome Analysis of Developing Seeds and Silique Wall Reveals Dynamic Transcription Networks for Effective Oil Production in *Brassica napus* L. *International Journal of Molecular Sciences*, 20(8):1982. 2019.
- E. Sifakis, et al. Elucidating the identity of resistance mechanisms to prednisolone exposure in acute lymphoblastic leukemia cells through transcriptomic analysis: A computational approach. *Journal of Clinical Bioinformatics*, 1. 2011.
- U. von Luxburg. A tutorial on spectral clustering. *Stat Comput*, 17(4):395–416. 2007.
- J. M. Wooldridge. *Econometric Analysis of Cross Section and Panel Data*. The MIT Press, 2010.

## A Proofs

### Proof of Proposition 2.1

We will denote the joint distribution of the fold changes pair  $\left[\widehat{\Gamma_i \circ \mathcal{W}_s}^\top \widehat{\Gamma_{i'} \circ \mathcal{W}_s}^\top\right]^\top$  in the following way:

$$\begin{bmatrix} \widehat{\Gamma_i \circ \mathcal{W}_s} \\ \widehat{\Gamma_{i'} \circ \mathcal{W}_s} \end{bmatrix} \sim \mathcal{N} \left( \begin{bmatrix} \Gamma_i \circ \mathcal{W}_s \\ \Gamma_{i'} \circ \mathcal{W}_s \end{bmatrix}, \begin{bmatrix} \Sigma_{\Gamma_i \circ \mathcal{W}_s} & P_{\Gamma_i \Gamma_{i'} \circ \mathcal{W}_s} \\ (P_{\Gamma_i \Gamma_{i'} \circ \mathcal{W}_s})^\top & \Sigma_{\Gamma_{i'} \circ \mathcal{W}_s} \end{bmatrix} \right).$$

Using Definitions 2.5 and 2.2, the means can be expressed depending on the warp type:

$$\begin{bmatrix} \Gamma_i \circ \mathcal{W}_s \\ \Gamma_{i'} \circ \mathcal{W}_s \end{bmatrix} = \begin{cases} \begin{bmatrix} \Gamma_i^{t_1} \dots \Gamma_i^{t_{p-s}} \Gamma_{i'}^{t_{1+s}} \dots \Gamma_{i'}^{t_p} \end{bmatrix}^\top & \text{if } s > 0 \\ \begin{bmatrix} \Gamma_i^{t_{1-s}} \dots \Gamma_i^{t_p} \Gamma_{i'}^{t_1} \dots \Gamma_{i'}^{t_{p+s}} \end{bmatrix}^\top & \text{if } s < 0 \\ [\Gamma_i^\top \Gamma_{i'}^\top]^\top & \text{if } s = 0 \end{cases},$$

Similarly, we can express the elements of the covariance matrix:

$$\Sigma_{\Gamma_i \circ \mathcal{W}_s} = \begin{cases} \begin{bmatrix} \sigma_{\Gamma_i^{t_1}}^2 & & 0 \\ & \ddots & \\ 0 & & \sigma_{\Gamma_i^{t_{p-s}}}^2 \end{bmatrix} & \text{if } s > 0 \\ \begin{bmatrix} \sigma_{\Gamma_i^{t_{1-s}}}^2 & & 0 \\ & \ddots & \\ 0 & & \sigma_{\Gamma_i^{t_p}}^2 \end{bmatrix} & \text{if } s < 0 \\ \Sigma_{\Gamma_i} & \text{if } s = 0 \end{cases}, \quad \Sigma_{\Gamma_{i'} \circ \mathcal{W}_s} = \begin{cases} \begin{bmatrix} \sigma_{\Gamma_{i'}^{t_{1+s}}}^2 & & 0 \\ & \ddots & \\ 0 & & \sigma_{\Gamma_{i'}^{t_p}}^2 \end{bmatrix} & \text{if } s > 0 \\ \begin{bmatrix} \sigma_{\Gamma_{i'}^{t_1}}^2 & & 0 \\ & \ddots & \\ 0 & & \sigma_{\Gamma_{i'}^{t_{p+s}}}^2 \end{bmatrix} & \text{if } s < 0 \\ \Sigma_{\Gamma_{i'}} & \text{if } s = 0 \end{cases}.$$

$$\text{and } K \circ \mathcal{W}_s = \begin{cases} \begin{bmatrix} 0 & & 0 \\ \vdots & \ddots & \vdots \\ \rho_{\Gamma_i \Gamma_{i'}^{t_1+s}} & & \\ 0 & \rho_{\Gamma_i \Gamma_{i'}^{t_p-s}} & 0 \end{bmatrix} & \text{if } s > 0 \\ \begin{bmatrix} 0 & \rho_{\Gamma_i \Gamma_{i'}^{t_1-s}} & 0 \\ \vdots & \ddots & \vdots \\ 0 & \rho_{\Gamma_i \Gamma_{i'}^{t_p+s}} & 0 \end{bmatrix} & \text{if } s < 0 \\ \Sigma_{\Gamma_{i'}} & \text{if } s = 0 \end{cases}$$

It can be noted that since the non-zero elements of the matrix  $K \circ \mathcal{W}_s$  have been moved from the diagonal to either sub-diagonal or super-diagonal of order  $s$ , its trace is now equal to zero. Since the condition on the joint distribution given in Definition 2.6 is satisfied, we can calculate the value of  $\widehat{\mathbf{diss}}_s$  element by element, starting with the square norm of the difference between means:

$$\|\Gamma_i \circ \mathcal{W}_s - \Gamma_{i'} \circ \mathcal{W}_s\|^2 = \begin{cases} \sum_{l=1}^{p-s} \left( \Gamma_i^{t_l} - \Gamma_{i'}^{t_l+s} \right)^2 & \text{if } s > 0 \\ \sum_{l=1-s}^p \left( \Gamma_i^{t_l} - \Gamma_{i'}^{t_l+s} \right)^2 & \text{if } s < 0 \\ \sum_{l=1}^p \left( \Gamma_i^{t_l} - \Gamma_{i'}^{t_l+s} \right)^2 & \text{if } s = 0 \end{cases} \quad .$$

Next, the trace of the covariance matrix of the first warped fold change in the pair:

$$\text{Tr}(\Sigma_{\Gamma_i} \circ \mathcal{W}_s) = \begin{cases} \sum_{l=1}^{p-s} \sigma_{\Gamma_i^{t_l}}^2 & \text{if } s > 0 \\ \sum_{l=1-s}^p \sigma_{\Gamma_i^{t_l}}^2 & \text{if } s < 0 \\ \sum_{l=1}^p \sigma_{\Gamma_i^{t_l}}^2 & \text{if } s = 0 \end{cases} \quad .$$

Similarly for the second fold change:

$$\text{Tr}(\Sigma_{\Gamma_{i'}} \circ \mathcal{W}_s) = \begin{cases} \sum_{l=1+s}^p \sigma_{\Gamma_i^{t_l}}^2 = \sum_{l=1}^{p-s} \sigma_{\Gamma_i^{t_{l+s}}}^2 & \text{if } s > 0 \\ \sum_{l=1}^{p+s} \sigma_{\Gamma_i^{t_l}}^2 = \sum_{l=1-s}^p \sigma_{\Gamma_i^{t_{l+s}}}^2 & \text{if } s < 0 \\ \sum_{l=1}^p \sigma_{\Gamma_i^{t_l}}^2 = \sum_{l=1}^p \sigma_{\Gamma_i^{t_{l+s}}}^2 & \text{if } s = 0 \end{cases} \quad .$$

Finally, the last term containing the cross-covariances is calculated:

$$\sum_{l=1}^{p-|s|} [\text{P}_{\Gamma_i \Gamma_{i'}} \circ \mathcal{W}_s]_{(l+s\mathbb{1}_{\mathbb{Z}_+^*}(s), l+s\mathbb{1}_{\mathbb{Z}_-^*}(s))} = \begin{cases} \sum_{l=1+s}^{p-s} \rho_{\Gamma_i \Gamma_{i'}}^{t_l} & \text{if } s > 0 \\ \sum_{l=1-s}^{p+s} \rho_{\Gamma_i \Gamma_{i'}}^{t_l} & \text{if } s < 0 \\ \sum_{l=1}^p \rho_{\Gamma_i \Gamma_{i'}}^{t_l} & \text{if } s = 0 \end{cases} \quad .$$

Hence, we obtain the value of the dissimilarity by writing the expression for any step  $s \in \mathbb{Z}$ .

□

## Proof of Proposition 2.2

Let  $(i, i') \in \{1, \dots, n_e\}^2$  be an entity pair. The statements of the proposition are equivalent to saying that, for any warp step  $s \in \mathcal{S}$ , we have:

$$\begin{cases} \min_{s \in \mathcal{S}} [\widehat{\text{diss}}_{\mathbf{s}}(\widehat{\Gamma_i \circ \mathcal{W}_s}, \widehat{\Gamma_{i'} \circ \mathcal{W}_s})] = \min_{s \in \mathcal{S}} [\widehat{\text{diss}}_{\mathbf{s}}(\widehat{\Gamma_{i'} \circ \mathcal{W}_s}, \widehat{\Gamma_i \circ \mathcal{W}_s})] \\ \arg \min_{s \in \mathcal{S}} [\widehat{\text{diss}}_{\mathbf{s}}(\widehat{\Gamma_i \circ \mathcal{W}_s}, \widehat{\Gamma_{i'} \circ \mathcal{W}_s})] = - \arg \min_{s \in \mathcal{S}} [\widehat{\text{diss}}_{\mathbf{s}}(\widehat{\Gamma_{i'} \circ \mathcal{W}_s}, \widehat{\Gamma_i \circ \mathcal{W}_s})] \end{cases} \quad . \quad (\text{A.1})$$

Let us denote  $s_* = \arg \min_{s \in \mathcal{S}} [\widehat{\text{diss}}_{\mathbf{s}}(\widehat{\Gamma_i \circ \mathcal{W}_s}, \widehat{\Gamma_{i'} \circ \mathcal{W}_s})]$ . To prove both parts of the proposition, it suffices to show that the following is true:

$$\widehat{\text{diss}}_{\mathbf{s}}(\widehat{\Gamma_i \circ \mathcal{W}_{s_*}}, \widehat{\Gamma_{i'} \circ \mathcal{W}_{s_*}}) = \widehat{\text{diss}}_{\mathbf{s}}(\widehat{\Gamma_{i'} \circ \mathcal{W}_{-s_*}}, \widehat{\Gamma_i \circ \mathcal{W}_{-s_*}}) \quad (\text{A.2})$$

Using the expression of the dissimilarity given in Proposition 2.1, we can develop the left-hand side of (A.2):

$$\widehat{\text{diss}}_{\mathbf{s}} \left( \widehat{\Gamma_i \circ \mathcal{W}_{s_*}}, \widehat{\Gamma_{i'} \circ \mathcal{W}_{s_*}} \right) = \sum_{l=l^*}^{p^*} \left( \Gamma_i^{t_l} - \Gamma_{i'}^{t_l+s_*} \right)^2 + \sum_{l=l^*}^{p^*} \sigma_{\Gamma_i^{t_l}}^2 + \sum_{l=l^*}^{p^*} \sigma_{\Gamma_{i'}^{t_l+s_*}}^2 - 2 \sum_{l=1+|s_*|}^{p-|s_*|} \rho_{\Gamma_i \Gamma_{i'}^{t_l}}. \quad (\text{A.3})$$

where  $l^* = 1 - s_* \mathbb{1}_{\mathbb{Z}_-^*}(s_*)$  and  $p^* = p - s_* \mathbb{1}_{\mathbb{Z}_+^*}(s_*)$ .

Similarly, we develop the right-hand side:

$$\widehat{\text{diss}}_{\mathbf{s}} \left( \widehat{\Gamma_{i'} \circ \mathcal{W}_{-s_*}}, \widehat{\Gamma_i \circ \mathcal{W}_{-s_*}} \right) = \sum_{l=l_*}^{p_*} \left( \Gamma_{i'}^{t_l} - \Gamma_i^{t_l-s_*} \right)^2 + \sum_{l=l_*}^{p_*} \sigma_{\Gamma_{i'}^{t_l}}^2 + \sum_{l=l_*}^{p_*} \sigma_{\Gamma_i^{t_l-s_*}}^2 - 2 \sum_{l=1+|-s_*|}^{p-|-s_*|} \rho_{\Gamma_{i'} \Gamma_i^{t_l}}. \quad (\text{A.4})$$

where  $l_* = 1 - (-s_*) \mathbb{1}_{\mathbb{Z}_-^*}(-s_*)$  and  $p_* = p - (-s_*) \mathbb{1}_{\mathbb{Z}_+^*}(-s_*)$ . These quantities can be rewritten as  $l_* = 1 + s_* \mathbb{1}_{\mathbb{Z}_+^*}(s_*) = l^* + s_*$  and  $p_* = p + s_* \mathbb{1}_{\mathbb{Z}_-^*}(s_*) = p^* + s_*$ . It can also be noticed that  $|-s_*| = |s_*|$ , and  $\rho_{\Gamma_{i'} \Gamma_i^{t_l}} = \rho_{\Gamma_i \Gamma_{i'}^{t_l}}$  by the symmetry of the covariance. Hence, we can rewrite (A.4) as follows:

$$\begin{aligned} \widehat{\text{diss}}_{\mathbf{s}} \left( \widehat{\Gamma_{i'} \circ \mathcal{W}_{-s_*}}, \widehat{\Gamma_i \circ \mathcal{W}_{-s_*}} \right) &= \sum_{l=l^*+s_*}^{p^*+s_*} \left( \Gamma_i^{t_l-s_*} - \Gamma_{i'}^{t_l} \right)^2 + \sum_{l=l^*+s_*}^{p^*+s_*} \sigma_{\Gamma_i^{t_l-s_*}}^2 \\ &\quad + \sum_{l=l^*+s_*}^{p^*+s_*} \sigma_{\Gamma_{i'}^{t_l}}^2 - 2 \sum_{l=1+|s_*|}^{p-|s_*|} \rho_{\Gamma_i \Gamma_{i'}^{t_l}}. \end{aligned} \quad (\text{A.5})$$

It can be noticed that the expression in (A.5) is identical to (A.3), which concludes the proof.

□

### Proof of Theorem 2.1

To prove the first statement, it suffices to show that the total cost always decreases, that is, for every iteration  $it$ ,  $TC_{it} \geq TC_{it+1}$ .

We denote  $(Cl_1, \dots, Cl_{n_e})$  and  $(Cl_1^*, \dots, Cl_{n_e}^*)$  cluster labels at iterations  $it$  and  $it + 1$

respectively. For a given initialization, the cost at iteration  $it$  can be written as follows:

$$TC_{it} = \sum_{k=1}^K \sum_{i \in cluster_k} \mathcal{OWD}_{iC_k}, \quad (\text{A.6})$$

given, for every cluster label  $k \in \{1, \dots, K\}$ ,  $cluster_k = \{i \in \{1, \dots, n_e\} | Cl_i = k\}$  the current composition of the cluster, and  $C_k$  the corresponding centroid. Similarly, the cost at iteration  $it + 1$  can be expressed:

$$TC_{it+1} = \sum_{k=1}^K \sum_{i \in cluster_k^*} \mathcal{OWD}_{iC_k^*}, \quad (\text{A.7})$$

given, for every cluster label  $k \in \{1, \dots, K\}$ ,  $cluster_k^* = \{i \in \{1, \dots, n_e\} | Cl_i^* = k\}$  the current composition of the cluster, and  $C_k^*$  the corresponding centroid. Additionally, for a given cluster label  $k$ , we denote the migrating sub-clusters:

- the sub-cluster of elements that left cluster  $k$  at  $it + 1$ :

$$cluster_k^{*C} = \{i \in \{1, \dots, n_e\} | Cl_i = k \text{ and } Cl_i^* \neq k\},$$

- the sub-cluster of elements that joined cluster  $k$  at  $it + 1$ :

$$cluster_k^C = \{i \in \{1, \dots, n_e\} | Cl_i \neq k \text{ and } Cl_i^* = k\}.$$

Noticing that  $cluster_k = (cluster_k^* \cup cluster_k^{*C}) \setminus cluster_k^C$ , the quantity  $TC_{it}$  can be decomposed as follows:

$$TC_{it} = \underbrace{\sum_{k=1}^K \sum_{i \in cluster_k^*} \mathcal{OWD}_{iC_k}}_A + \underbrace{\sum_{k=1}^K \sum_{i \in cluster_k^{*C}} \mathcal{OWD}_{iC_k}}_B - \underbrace{\sum_{k=1}^K \sum_{i \in cluster_k^C} \mathcal{OWD}_{iC_k}}_C. \quad (\text{A.8})$$

First, it follows from the "Update" step by construction that

$$A = \sum_{k=1}^K \sum_{i \in cluster_k^*} \mathcal{OWD}_{iC_k} \geq \sum_{k=1}^K \sum_{i \in cluster_k^*} \mathcal{OWD}_{iC_k^*} = TC_{it+1}.$$

Next, we consider the quantities B and C. It can be noticed, by construction of the "Assign" step, that for every  $i \in cluster_k^{*C}$  there exists a unique  $k^* \in \{1, \dots, K\} \setminus k$  such that  $i \in cluster_{k^*}^C$  and  $\mathcal{OWD}_{iC_{k^*}} \leq \mathcal{OWD}_{iC_k}$ . In other words, there is a bijection between the indices in B and C, such that the corresponding elements of the sum in B are larger than those in C. Therefore,  $B - C \geq 0$ , and  $TC_{it} = A + B - C \geq TC_{it+1}$ .

Thus, the total cost sequence is decreasing, and, noticing that total cost is positive, it can be concluded that the sequence has a limit. Finally, there is a finite number of cluster configurations possible, therefore the sequence of total costs contains a finite number of values. Hence, the algorithm converges in a finite number of iterations.

The second statement follows directly from Definitions 2.7 and 2.8. In particular, we have:

- Line 12 of Algorithm 2 is equivalent to lines 11-19 of Algorithm 1, since:

$$\arg \min_{k \in \{1, \dots, K\}} \mathcal{OWD}_{iC_k} = \arg \min_{k \in \{1, \dots, K\}} \left( \min_{s \in \mathcal{S}} \left[ \widehat{\text{diss}}_s \left( \widehat{\Gamma_i \circ \mathcal{W}_s}, \widehat{\Gamma_{C_k} \circ \mathcal{W}_s} \right) \right] \right) = \arg \min_{k \in \{1, \dots, K\}} (d_k),$$

where  $d_k$  is the quantity from Algorithm 1 of the final value after the for loop terminating at line 19.

- Lines 18-22 of Algorithm 2 are equivalent to lines 25-33 of Algorithm 1, since:

$$\sum_{i' \in cluster_k} \mathcal{OWD}_{ii'} = \sum_{i' \in cluster_k} \mathcal{OWD}_{i'i} = \sum_{i' \in cluster_k} \widehat{\text{diss}}_s \left( \widehat{\Gamma_{i'} \circ \mathcal{W}_s}, \widehat{\Gamma_i \circ \mathcal{W}_s} \right),$$

due to the symmetry of  $\mathcal{OWD}$ , the final quantity being equivalent to the value of  $d_{cluster_k}$  at line 33 of Algorithm 1.

- Line 37 of Algorithm 2 is equivalent to line 48 of Algorithm 1.

We obtain the following complexities for different parts of the algorithms:

- 1. Assign step:**  $\mathcal{O}(n_e K |\mathcal{S}|)$  for Algorithm 1, and  $\mathcal{O}(n_e K)$  for Algorithm 2.
- 2. Update step:**  $\mathcal{O}(n_e^2 K |\mathcal{S}|)$  for Algorithm 1, and  $\mathcal{O}(n_e^2 K)$  for Algorithm 2.

Thus, adding the complexity of calculating the matrices  $\mathcal{OWD}$  and  $\mathcal{OW}$  beforehand, we obtain in total  $\mathcal{O}(n_{init} it_{max} n_e K |\mathcal{S}| (1 + n_e))$  for Algorithm 1, and  $\mathcal{O}(n_{init} it_{max} n_e K (1 + n_e) + n_e^2 |\mathcal{S}|)$  for Algorithm 2. The degree of the largest polynomial of the former is 6, and that of the latter is 5, hence Algorithm 2 is less complex.  $\square$

## B Data preprocessing

Before performing clustering, certain transformations have to be applied to the raw data in order to amplify those characteristics that are of particular interest, and reduce those that can be ignored. We perform data scaling with respect to the following criteria:

- **Scaling by standard deviation:** performed in order to account for uncertainties, so that the observations with high uncertainty caused by individual variability appear with lower weight compared to those with low uncertainty. Standard deviation estimates are calculated as follows: for  $i \in \{1, 2, \dots, n_e\}$  we denote  $\sigma_{\Gamma_i} = (\sigma_{\Gamma_i^{t_1}}, \dots, \sigma_{\Gamma_i^{t_p}})$  where  $\sigma_{\Gamma_i^{t_l}} = \sqrt{\sigma_{\Gamma_i^{t_l}}^2}$ .
- **Scaling by the fold change norm:** performed with the purpose of diminishing the effect of scale differences between the fold changes. The norm of  $\hat{\Gamma}_i$  associated with the distance  $\widehat{\mathbf{d}}_2^2$  or the dissimilarity  $\widehat{\mathbf{diss}}_s$  can be expressed as follows:

$$Norm(\hat{\Gamma}_i) = \sqrt{\|\Gamma_i\|_2^2 + \text{Tr}(\Sigma_{\Gamma_i})} = \sqrt{\|\Gamma_i\|_2^2 + \sum_{l=1}^p \sigma_{\Gamma_i^{t_l}}^2}. \quad (\text{B.1})$$



The two scaling transformations described above are applied in a consecutive manner: the fold change norm scaling is calculated based on the result of the scaling by standard deviation, which implies that the norm of the final output is equal to 1. Thus, we obtain a processed dataset, from which new pairs of random fold changes estimators are constructed, and finally the pairwise distances are calculated. An illustrative example for the effect of preprocessing on the fold changes can be found in Figure C.2.

## B.1 Fold change estimation from preprocessed data

After applying the preprocessing to the response  $Y_{ikj}^t$  of an entity  $i$  at the time point  $t$  for a replicate  $j$  under the experimental condition  $k$ , the response becomes:

$$\tilde{Y}_{ikj}^t = \frac{Y_{ikj}^t}{\sigma_{\Gamma_i^t} \times \text{Norm}(\Sigma_{\Gamma_i}^{-1} \hat{\Gamma}_i)}, \text{ where } \sigma_{\Gamma_i^t} = \sqrt{\sigma_{\Gamma_i^t}^2}. \quad (\text{B.2})$$

We obtain the following expression by applying the norm defined in (B.1) to the fold change  $\hat{\Gamma}_i$  after the scaling by standard deviation:

$$\text{Norm}(\Sigma_{\Gamma_i}^{-1} \hat{\Gamma}_i) = \sqrt{\sum_{l=1}^p \left[ \left( \frac{\Gamma_i^{t_l}}{\sigma_{\Gamma_i^{t_l}}^2} \right)^2 + 1 \right]}. \quad (\text{B.3})$$

The joint distribution of a fold change pair obtained from the preprocessed data can be rewritten in the following way:

$$\begin{bmatrix} \hat{\Gamma}_i \\ \hat{\Gamma}_{i'} \end{bmatrix} \sim \mathcal{N} \left( \begin{bmatrix} \tilde{\Gamma}_i \\ \tilde{\Gamma}_{i'} \end{bmatrix}, \begin{bmatrix} \Sigma_{\tilde{\Gamma}_i} & P_{\tilde{\Gamma}_i \tilde{\Gamma}_{i'}} \\ (P_{\tilde{\Gamma}_i \tilde{\Gamma}_{i'}})^\top & \Sigma_{\tilde{\Gamma}_{i'}} \end{bmatrix} \right) \text{ such that:}$$

- Means for  $x \in \{i, i'\}$ :

$$\begin{aligned}\tilde{\Gamma}_x &= \left( \frac{\sum_{j=1}^{n_r} (Y_{i1j}^{t_1} - Y_{i0j}^{t_1})}{n_r \sigma_{\Gamma_x^{t_1}} \text{Norm}(\Sigma_{\Gamma_x}^{-1} \hat{\Gamma}_x)}, \dots, \frac{\sum_{j=1}^{n_r} (Y_{i1j}^{t_p} - Y_{i0j}^{t_p})}{n_r \sigma_{\Gamma_x^{t_p}} \text{Norm}(\Sigma_{\Gamma_x}^{-1} \hat{\Gamma}_x)} \right) \\ &= \frac{1}{\text{Norm}(\Sigma_{\Gamma_x}^{-1} \hat{\Gamma}_x)} \left( \frac{\Gamma_x^{t_1}}{\sigma_{\Gamma_x^{t_1}}}, \dots, \frac{\Gamma_x^{t_p}}{\sigma_{\Gamma_x^{t_p}}} \right),\end{aligned}\tag{B.4}$$

- Covariance matrices for  $x \in \{i, i'\}$ :  $\Sigma_{\tilde{\Gamma}_x} = \begin{bmatrix} \sigma_{\tilde{\Gamma}_x^{t_1}}^2 & & 0 \\ & \ddots & \\ 0 & & \sigma_{\tilde{\Gamma}_x^{t_p}}^2 \end{bmatrix},$

$$\begin{aligned}\text{with } \sigma_{\tilde{\Gamma}_x^t}^2 &= \frac{\sum_{j=1}^{n_r} \left[ (\tilde{Y}_{i1j}^t - \overline{\tilde{Y}_{i1}^t})^2 + (\tilde{Y}_{i0j}^t - \overline{\tilde{Y}_{i0}^t})^2 \right]}{n_r - 1} = \frac{\sigma_{\Gamma_x^t}^2}{\sigma_{\Gamma_x^t}^2 \left( \text{Norm}(\Sigma_{\Gamma_x}^{-1} \hat{\Gamma}_x) \right)^2} \\ &= \frac{1}{\left( \text{Norm}(\Sigma_{\Gamma_x}^{-1} \hat{\Gamma}_x) \right)^2}.\end{aligned}\tag{B.5}$$

- Cross-covariance matrix:  $P_{\tilde{\Gamma}_i \tilde{\Gamma}_{i'}} = \begin{bmatrix} \rho_{\tilde{\Gamma}_i^{t_1} \tilde{\Gamma}_{i'}^{t_1}} & & 0 \\ & \ddots & \\ 0 & & \rho_{\tilde{\Gamma}_i^{t_p} \tilde{\Gamma}_{i'}^{t_p}} \end{bmatrix},$

$$\begin{aligned}\text{with } \rho_{\tilde{\Gamma}_i^t \tilde{\Gamma}_{i'}^t} &= \frac{\sum_{j=1}^{n_r} \left[ (\tilde{Y}_{i1j}^t - \overline{\tilde{Y}_{i1}^t})(\tilde{Y}_{i'1j}^t - \overline{\tilde{Y}_{i'1}^t}) + (\tilde{Y}_{i0j}^t - \overline{\tilde{Y}_{i0}^t})(\tilde{Y}_{i'0j}^t - \overline{\tilde{Y}_{i'0}^t}) \right]}{n_r - 1} \\ &= \frac{\rho_{\Gamma_i^t \Gamma_{i'}^t}}{\sigma_{\Gamma_{i'}^t} \sigma_{\Gamma_i^t} \text{Norm}(\Sigma_{\Gamma_i}^{-1} \hat{\Gamma}_i) \text{Norm}(\Sigma_{\Gamma_{i'}}^{-1} \hat{\Gamma}_{i'})}.\end{aligned}\tag{B.6}$$

## C Supplementary figures

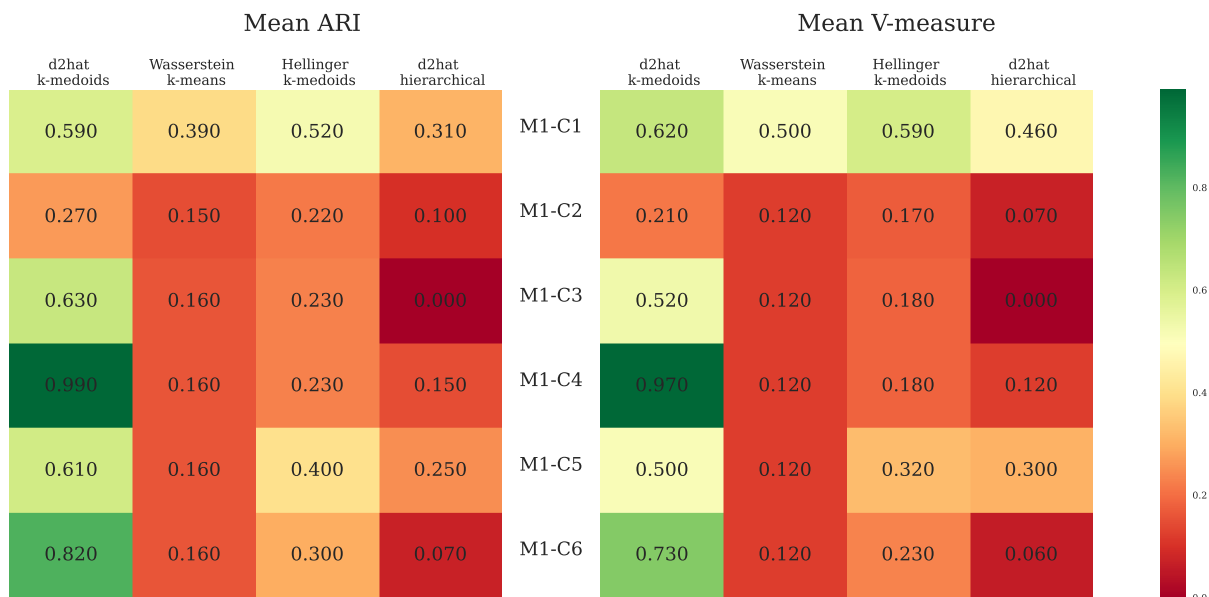


Figure (C.1) Results of the simulation study comparing distances and clustering algorithms.

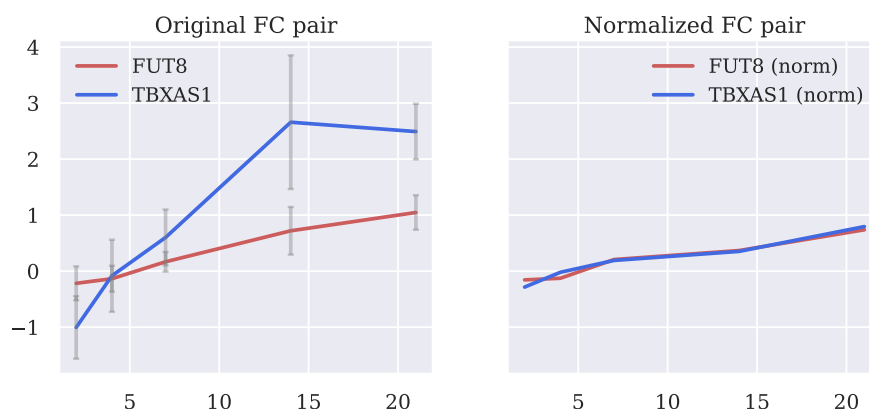


Figure (C.2) The effect of raw data scaling illustrated on a figure, where means with standard deviation of a pair of transcriptomic fold changes are plotted, inferred from the original data on the left and from scaled data on the right. As a result of scaling, the fold changes of genes *TBXAS1* and *FUT8* are rendered significantly closer than the original. For instance, it can be observed that the original fold changes are both characterized by almost monotonous growth during the whole period after irradiation. On the one hand, the curve of gene *TBXAS1* is more concave, which can be neglected, and the difference is reduced by the scaling with respect to the norm. On the other hand, the scaling with respect to the standard deviation reduces the peak in the mean of gene *TBXAS1* observed at day 14, which is also negligible due to very high standard deviation at that point.

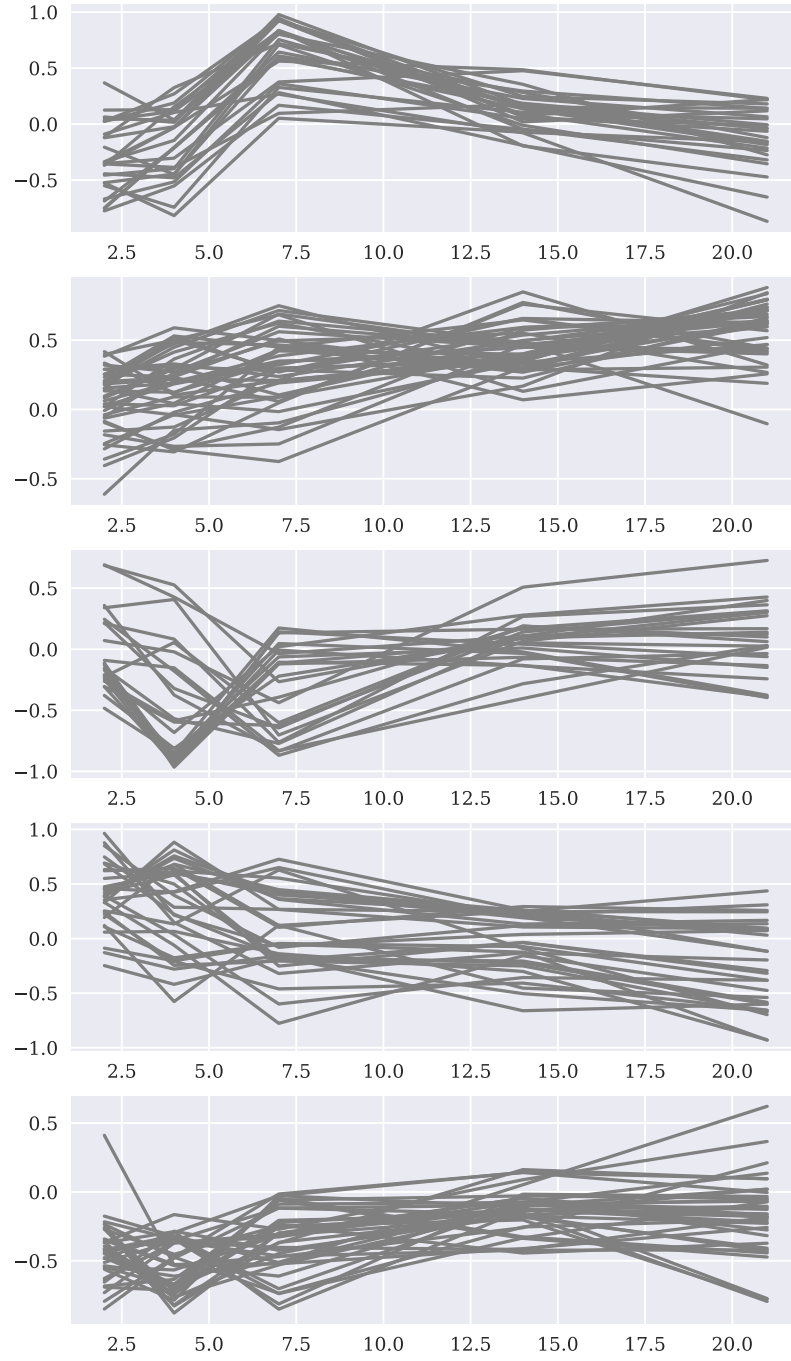


Figure (C.3) Means of the fold changes in each of the 5 clusters obtained as a result of the clustering of the LINAC dataset with  $\mathcal{O}WD$ -based spectral clustering. The order of clusters is chosen to maximize the pairwise intersections with the clusters presented in Figure 4.1.

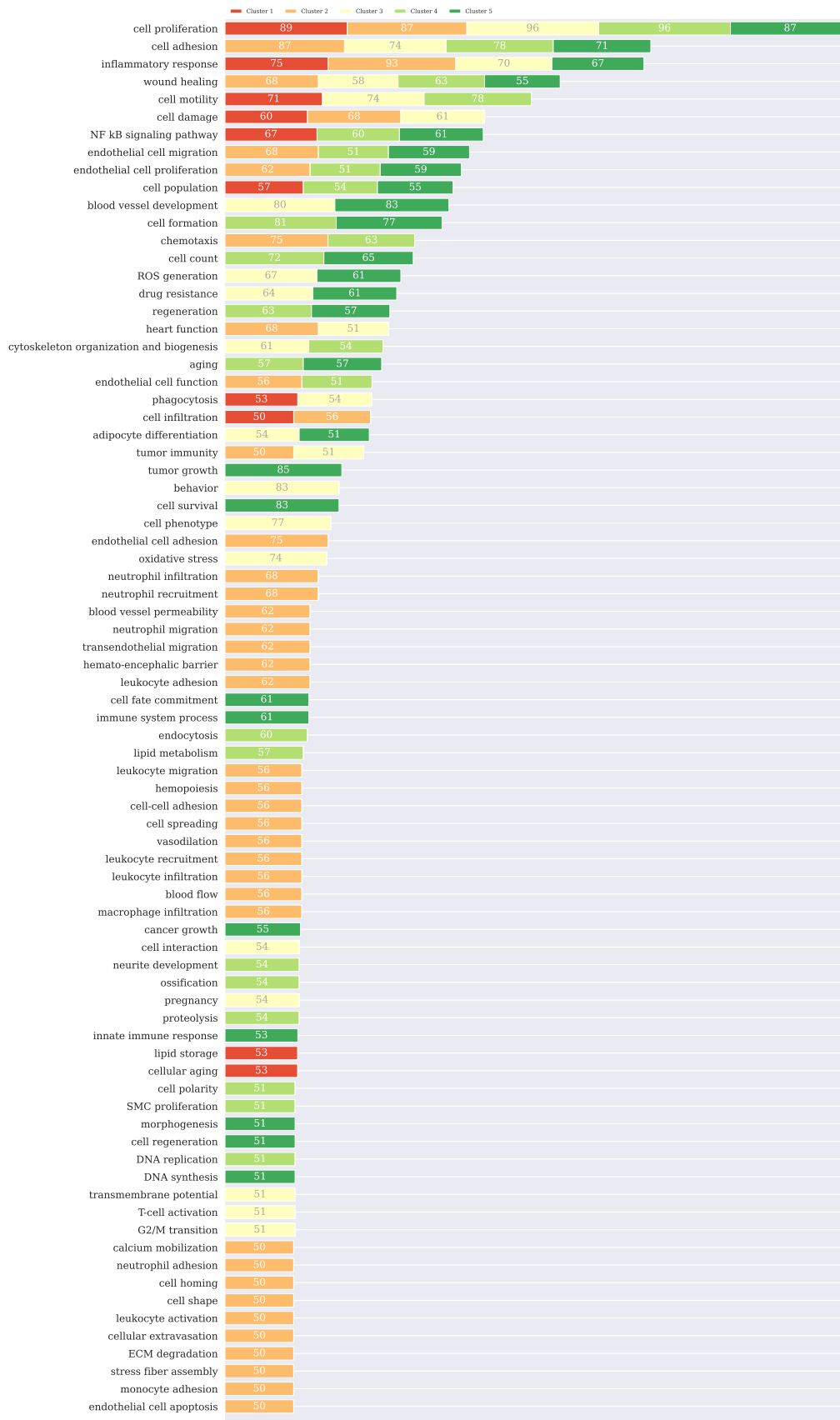


Figure (C.4) Summary of the enrichment with cellular processes of the clusters obtained for the LINAC dataset. Cellular processes, listed on the left, are sorted from the most represented to the least. The enriched clusters are indicated with different colors. The numbers on the bars indicate the percentage of overlap with the given process for the given cluster.